Flowfield Simulation and Performance Prediction of Electrothermal Pulsed Plasma Thrusters onboard Osaka Institute of Technology PROITERES Nano-Satellite Series

IEPC-2015-207／ISTS-2015-b-207

Presented at Joint Conference of 30th International Symposium on Space Technology and Science
34th International Electric Propulsion Conference and 6th Nano-satellite Symposium,
Hyogo-Kobe, Japan
July 4 – 10, 2015

Ryota Fujita[1], Rikio Muraoka[2], Keita Kanaoka[3], Chen Huanjun[4], Masato Tanaka[5] and Hirokazu Tahara[6]
Osaka Institute of Technology, Asahi-ku, Osaka 535-8585, Japan

and

Takashi Wakizono[7]
High Serve Inc., Akiruno, Tokyo 190-0152, Japan

Abstract: The Project of Osaka Institute of Technology Electric-Rocket-Engine onboard Small Space Ship (PROITERES) was started at Osaka Institute of Technology (OIT) in 2007. In the 1st PROITERES, a nano-satellite with electrothermal-acceleration-type Pulsed Plasma Thrusters (PPTs) was successfully launched on September 9th, 2012. The main mission is to change an orbital altitude of 1 km by powered-flight with PPT systems. The PPT performance in the 1st PROITERES reached 5.0 Ns with no miss-firing. Furthermore, the project of the 2nd PROITERES was started in 2010. The 2nd PROITERES satellite aims at powered-flight with longer distance, i.e. changing 200-400 km in altitude on near-earth orbits, than that of the 1st PROITERES. In this paper, we numerically simulated flowfield in electrothermal PPTs, and evaluated their performance. We changed resistance values of the electric circuit of 0.005, 0.01 and 0.024 Ω. The results showed that the maximum impulse bit was 2,260 µNs at the lowest resistance value of 0.005 Ω.

Nomenclature

ε_0	=	permittivity of vacuum
R	=	electric resistance
L	=	electric inductance
C	=	capacitance
r	=	radial coordinate

[1] Graduate Student, Major in Mechanical Engineering, Graduate School of Engineering, and m1m14416@st.oit.ac.jp.
[2] Graduate Student, Major in Mechanical Engineering, Graduate School of Engineering, and tahara@med.oit.ac.jp.
[3] Graduate Student, Major in Mechanical Engineering, Graduate School of Engineering, and m1m15409@st.oit.ac.jp.
[4] Graduate Student, Major in Mechanical Engineering, Graduate School of Engineering, and tahara@med.oit.ac.jp.
[5] Graduate Student, Major in Mechanical Engineering, Graduate School of Engineering, and tahara@med.oit.ac.jp.
[6] Professor, Department of Mechanical Engineering, Faculty of Engineering, and tahara@med.oit.ac.jp.
[7] Researcher, Electric Propulsion R&D Section, and wakizon@kch.biglobe.ne.jp.

z = axial coordinate
t = time
e = total energy per unit volume
k = boltzmann factor or heat conductivity
h = planck constant
m = mass
q = heat flux
a = energy accommodation coefficient
σ = collision cross section

Index
c = capacitor
e = electron
h = baryon (ion and neutral)
i = ion
n = neutral
p = plasma
s = surface
w = wall
tran = transmission
conv = convection
cond = conduction

I. Introduction

In recent years, researchers are take interest in a nano-satellites by cutting of launching cost and shortening of development period. The project of Osaka Institute of Technology Electric-Rocket-Engine onboard Small Space Ship (PROITERES), as shown in Fig. 1, was started at Osaka Institute of Technology (OIT) in 2007[1-7]. In 1st PROITERES, a nano-satellite with electrothermal-acceleration-type Pulsed Plasma Thrusters (PPTs) was successfully launched by the Indian PSLV C-21 rocket on September 9th, 2012, as shown in Figs. 2 and 3, and Table 1. The main mission is to change orbital altitude of 1 km as powered-flight by PPT systems and to observe Kansai district in Japan with a high-resolution camera. Furthermore, the project of the 2nd PROITERES was started in 2010, as shown in Fig. 4 and Table 2. The 2nd PROITERES satellite aims at powered-flight with longer distance, i.e. changing 200-400 km in altitude on near-earth orbits, than that of the 1st PROITERES.

In this study, we examined the design criteria from results of numerical calculation of high-power PPT systems onboard the 2nd PROITERES satellite, and it was compared experimental results.

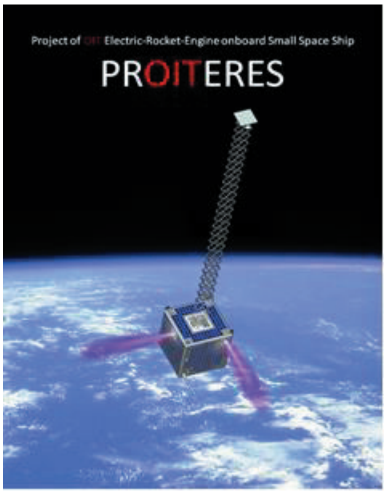

Figure 1. PROITERES satellite image during orbit.

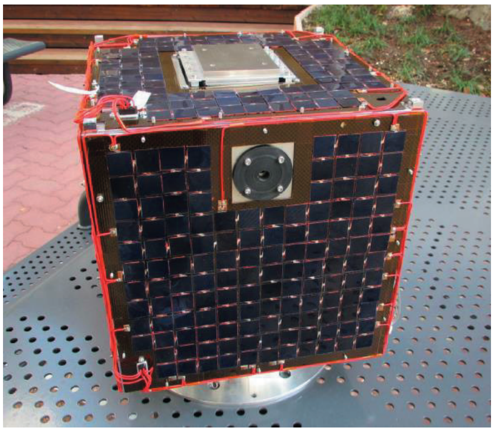

Figure 2. The 1st PROITERES satellite Flight Model.

Figure 3. Launch of PSLV C-21 rocket on Sept. 9th 2012.

Table 1. Specification of the 1st PROITERES satellite.

Mass	14.5 kg
Outside dimension	290 x 290 x 290 mm (Without extension boom)
Orbit	Orbital inclination: 99.98 deg, Eccentricity：0
Altitude	670 km
Commencing time	Apr. 2007
Life time	1-2 years
Rocket	PSLV(India)
Launch	Sept. 9 th.2012
Attitude control	Magnetic attitude control Gravity-gradient stabilization

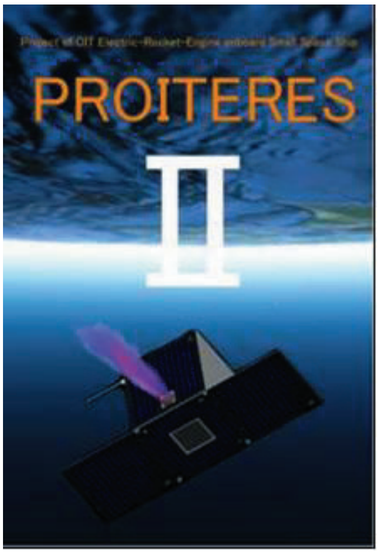

Figure 4. Illustration of the 2nd PROITERES satellite.

Table 2. Specification of the 2nd PROITERES satellite.

Mass	50 kg
Outside dimension	500 x 500 x 500 mm (Without extension boom)
Orbit	Orbitalinclination:99.98 deg, Eccentricity：0
Altitude	670 km
Commencing time	2010
Life time	1-2 years
Attitude control	Magnetic attitude control Gravity-gradient stabilization

II. Electrothermal PPT Systems

A propellant of the PPT is PTFE (polytetrafluoroethylene: Teflon®) of a solid propellant, and our PPT is a repetitively-pulsed-operation electric thruster[8-9]. Also, it is composed by two electrodes, the solid propellant, ignitor, capacitance and power supply systems for ignition and main discharges. The PPT has some features superior to other electric thruster. It has no sealing part, simple structure and high reliability, which are benefits by using the solid propellant, mainly the PTFE. The PPT has two types of an electrothermal-acceleration-type and an electromagnetic-acceleration-type, as shown in Figs. 5 and 6. The electrodes of the electrothermal-acceleration-type PPT are constructed coaxially. The electrodes of the electromagnetic-acceleration-type PPT are constructed parallelly.

We describe the operating principle of PPT. Firstly, high voltage charging in the capacitance by power supply for main discharge is conducted. Secondly, the propellant surface is ablated by ignition discharge. Then, an area of high conductivity is generated between the electrodes. Thirdly, the high voltage of the main capacitance was applied between the electrodes, and main discharge is started. The plasma which is generated by main discharge is accelerated electrothermally or electromagnetically.

The electrothermal-acceleration-type and the electromagnetic-acceleration-type, respectively, have good and bad events. We have studied the electrothermal-acceleration-type PPT, which generally had higher thrust-to-power ratios (an impulse bit per unit initial energy stored in the capacitors) and higher thrust efficiency than the electromagnetic-acceleration-type PPT. Although the electrothermal-acceleration-type PPT has lower specific impulse than the electromagnetic-acceleration-type PPT, the low specific impulse is not a significant problem as long as the PPT uses the solid propellant because there is no need to mount tank and valve which would be a large weight system.

At OIT, the project of the 2nd PROITERES was started in 2010. The 2nd PROITERES satellite aims at powered-flight with longer distance, i.e. changing 200-400 km in altitude on near-earth orbits, than that of the 1st PROITERES. We are developing a high-power and a high-total-impulse PPT systems.

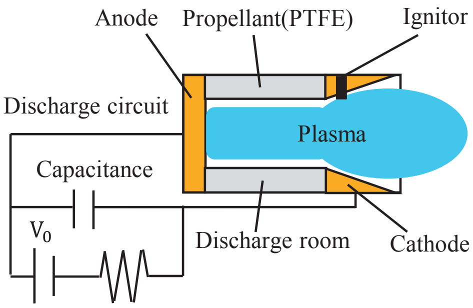

Figure 5. Electrothermal-acceleration-type PPT.

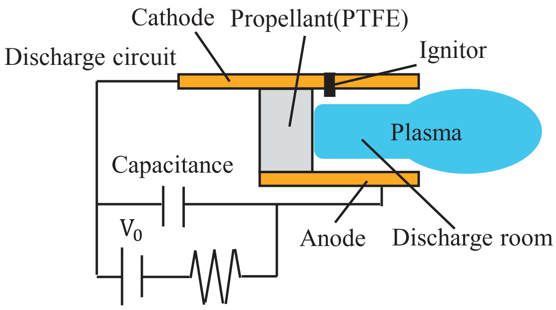

Figure 6. Electromagnetic-acceleration-type PPT.

III. Experimental Facility

Figure 7 shows the thrust stand in the vacuum chamber for precise measurement of the thrust of the PPT. The PPT and the capacitors are mounted on the pendulum, which rotates around fulcrums of two knife edges without friction. The displacement of the pendulum is measured by an eddy-current-type gap sensor (non-contacting micro-displacement meter) near the PPT. The electromagnetic damper is used to suppress mechanical noises and to decrease quickly the amplitude for the next measurement after operating the PPT. It is useful for a sensitive the thrust stand because it is non-contacting. The damper consists of a permanent magnet fixed to the pendulum and two coils fixed to the supporting stand. The control circuit differentiates the output voltage of the displacement sensor and supplies the current proportional to the differentiated voltage to the coil. Accordingly, the damper acts as a viscosity resistor. The damper is turned off just before operating the PPT for measurements without damping, and turned on after the measurement to prepare for the next measurement.

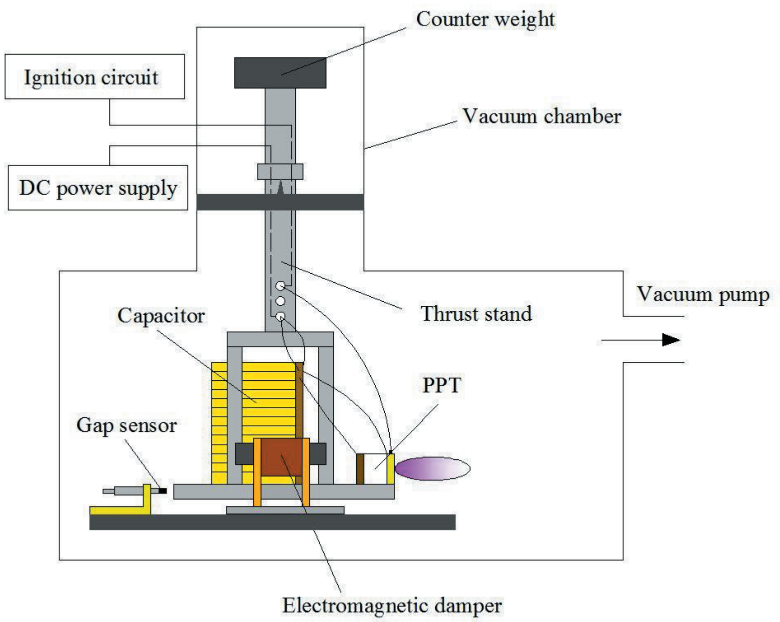

Figure 7. Thrust stand installed in the vacuum chamber.

Figure 8 shows the vacuum chamber 1.25 m in length and 0.6 m in inner diameter, which is evacuated using a turbo-molecular pump with a pumping speed of 3,000 l/s. The pressure is kept below 1.0x10^{-2} Pa during the PPT operation.

Figure 8. Vacuum chamber.

IV. Numerical calculation

A. Numerical calculation model

The PPT discharge terminates in few tens of μs or less. Therefore, physical quantity is difficult to measurement by the experiment. This study aims to elucidate the physical phenomena in a discharge room with two-dimertional area by the numerical calculation. An unsteady numerical calculation is carried out to predict performance in the PPT discharge system including plasma and discharge electric circuit. Figure 9 shows the calculation model of the PPT system. The calculation simultaneously simulates unsteady phenomena of discharge in the circuit, heat transfer to the PTFE, heat conduction inside the PTFE, ablation from the PTFE surface and plasma flow. The calculation domain of the discharge chamber, as shown in Fig. 10, in the nozzle cathode and in the cylindrical cavity made of PTFE. The length and diameter of the cavity are changed considering operational conditions[10-12].

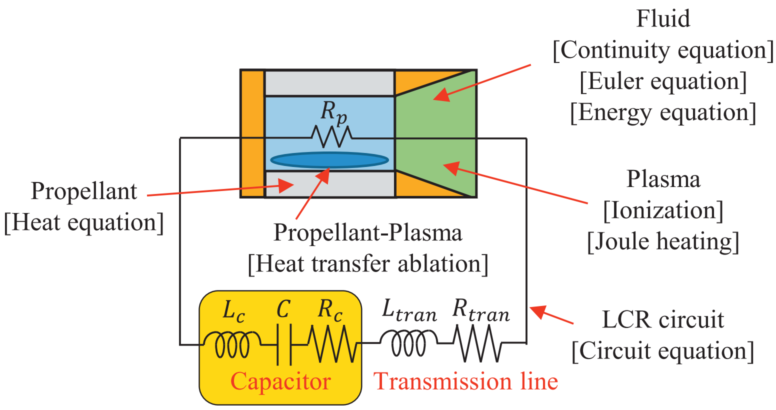

Figure 9. Numerical calculation model of the PPT system.

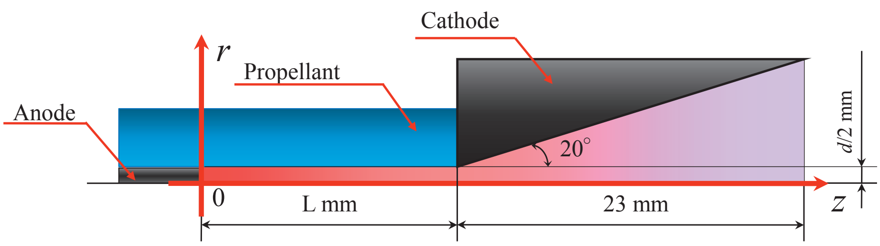

Figure 10. Numerical calculation domain.

B. Equations and boundary conditions

The Axisymmetric two-dimensional unsteady flowfield equations, conservation equations of mass, momentum and energy, are shown as follows.

Mass:

$$\frac{\partial}{\partial t}\rho+\frac{\partial}{\partial r}M_r+\frac{\partial}{\partial z}M_z=-\frac{1}{r}M_r \tag{1}$$

Momentum (Euler Eqs.):

r-direction:

$$\frac{\partial}{\partial t}M_r+\frac{\partial}{\partial r}\left[\frac{{M_r}^2}{\rho}+p\right]+\frac{\partial}{\partial Z}\left[\frac{M_r M_z}{\rho}\right]=-\frac{1}{r}\frac{{M_r}^2}{\rho} \tag{2}$$

z-direction:

$$\frac{\partial}{\partial t}M_z+\frac{\partial}{\partial r}\left[\frac{M_r M_z}{\rho}\right]+\frac{\partial}{\partial z}\left[\frac{{M_z}^2}{\rho}+p\right]=-\frac{1}{r}\frac{M_r M_z}{\rho} \tag{3}$$

Energy:

$$\frac{\partial}{\partial t}e+\frac{\partial}{\partial r}\left[\frac{M_r}{\rho}(e+p)\right]+\frac{\partial}{\partial z}\left[\frac{M_z}{\rho}(e+p)\right]=-\frac{1}{r}\frac{M_r}{\rho}(e+p)+Q_j \tag{4}$$

where ρ, p, and e are density, pressure and internal energy of flow, respectively, and M_r and M_z are momentum fluxes of raidial and axial directions, respectively. Q_j is Joule heat. Ionization equilibrium is assumed as follows.

Saha equation:

$$\frac{\alpha^2}{1-\alpha^2}=2.6\frac{(kT)^{5/2}(2\pi m_e)^{3/2}}{ph^3}\exp\left(-\frac{qE_i}{kT}\right) \tag{5}$$

where α and T are degree of ionization and temperature of flow, respectively, and E_i is corresponding voltage of ionization, in which the average ionization voltage of PTFE decomposed atoms (carbon and hydrogen etc.) are used.

The Joule heat is written as follows:

$$Q_j=\rho_p j^2 \tag{6}$$

$$\rho_p=\frac{\ln\Lambda}{1.53\times10^{-2}T^{3/2}}+\frac{m_e}{n_e e^2}\cdot\sigma_{e-n}n_n\left(\frac{3kT}{m_e}\right)^{1/2}$$

$$\ln\Lambda=\ln[12\pi n_e\left(\varepsilon_0 kT/e^2\, n_e\right)^{3/2}]$$

where ρ_p is electric resistance corresponding electron-ion and electron-neutral collisions, in which n_e and n_n are densities of electron and neutral, respectively, and j is current density in axial direction.

Figure 11 shows the model of heat fluxes from plasma to PTFE surface in the cavity, and their heat fluxes and the interaction are written as follows.

Heat convection:

$$q_{h,conv}=a_i(\varphi_i+\varphi_n)\cdot 2k(T_{h,w}-T_s) \tag{7}$$

Heat conduction:

$$q_{h,cond}=k\frac{\partial T_{h,w}}{\partial r} \tag{8}$$

Interaction equation:

$$q_{h,conv}=q_{h,cond} \tag{9}$$

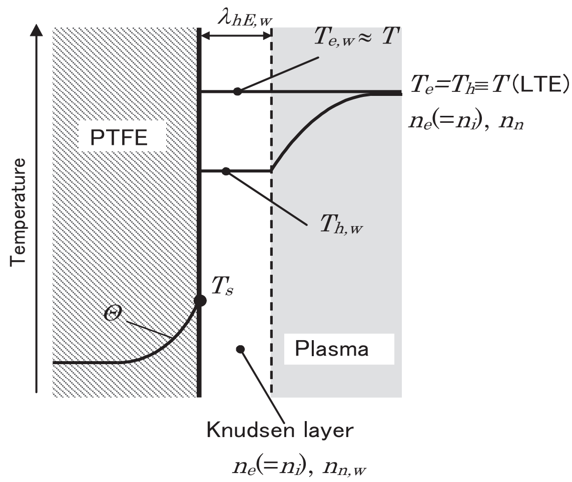

Figure 11. Heat transfer inside PTFE.

where φ_i and φ_n are particle number fluxes of ion and neutral, respectively, to PTFE surface. In evaporation of PTFE on the cavity wall, we uses the following equations.

Langmuir's law:

$$\Gamma = \left(\frac{m_n}{2\pi k T_s} \right)^{1/2} p_{vap} \tag{10}$$

$$p_{vap} = p_c \exp(-T_c / T_s)$$

$$p_c = 1.84 \times 10^{15}, \qquad T_c = 20815K$$

Evaporation heat flux:

$$q_{ab} = \frac{\Gamma}{m_n} \cdot 2kT_s \tag{11}$$

where Γ and q_{ab} are mass and heat fluxes, respectively, from PTFE surface, and p_{va} and T_s are evaporation pressure and PTFE surface temperature, respectively.

In heat conduction inside the PTFE block, the heat conduction equation and the boundary condition are written as follows.

$$\frac{\partial \Theta}{\partial t} = \frac{\kappa}{\rho_{PTFE} C_p} \left(\frac{\partial^2 \Theta}{\partial r'^2} + \frac{1}{r'} \frac{\partial \Theta}{\partial r'} + \frac{\partial^2 \Theta}{\partial z^2} \right) \tag{12}$$

$$\kappa \frac{\partial \Theta}{\partial r} \Big|_{r=0} = \left(Q_{conv} - Q_{ab} \right)$$

where Θ is temperature inside the PTFE. Finally, we close the equation system by using the following electric circuit equation.

From Fig. 9:

$$\left(L_{tran} + L_c \right) \ddot{Q} + \left(R_{tran} + R_c + R_p \right) \dot{Q} + \frac{Q}{C} = 0 \tag{13}$$

$$J = -\dot{Q}$$

Initial condition:

$$Q_0 = CV_0$$

After all equations were normalized, the flowfield equations are numerically solved by TVD-MacCormack scheme and average of Roe. In the calculation process, the electric circuit equation is solved by Runge-Kutta method, and the axial current density is obtained. The boundary conditions shown in Fig. 12 are assumed. For calculation start, a very low density plasma is distributed just before the calculation. The calculation grid sizes are 0.5 mm in axial direction and 0.025 mm in radial direction, and the time step is 10^{-9} s.

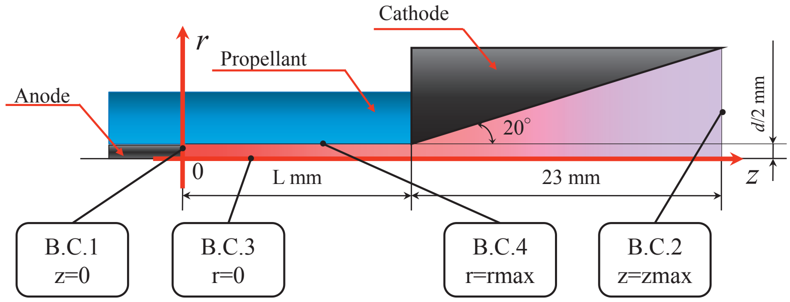

	ρ	M_r	M_z	e
B.C.1	$\frac{\partial \rho}{\partial z}=0$	$\frac{\partial M_r}{\partial z}=0$	$M_z=0$	$\frac{\partial e}{\partial z}=0$
B.C.2	$\frac{\partial \rho}{\partial z}=0$	$\frac{\partial M_r}{\partial z}=0$	$\frac{\partial M_z}{\partial z}=0$	$\frac{\partial e}{\partial z}=0$
B.C.3	$\frac{\partial \rho}{\partial r}=0$	$M_r=0$	$\frac{\partial M_z}{\partial r}=0$	$\frac{\partial e}{\partial r}=0$
B.C.4	$\Delta\rho_r=\rho_{ab}$	$M_r=\Gamma$	$\frac{\partial M_z}{\partial r}=0$	$\Delta e_r=Q_{ab}-Q_{conv}$

Figure 12. Boundary conditions.

C. Calculation assumptions

We assumed the following items about the numerical calculation.

1. Plasma flow was considered to be a non-viscous fluid. And, plasma flow was defined as an ideal gas.
2. Local thermal equilibrium was established in the plasma gas. Namely, they were assumed to be equal to the electron temperature, ion temperature, and the neutral particle temperature. However, it is not established in near the surface of the solid propellant.
3. In this case, ionization considered only monovalent ionization. And, plasma is in ionization equilibrium state.
4. These does not consider the influence of the magnetic field and the electric field.
5. Impedance of the plasma has only the DC resistance component.
6. RLC discharge circuit is considered the series circuit including the resistance of the non-stationary plasma. And, DC resistance of the circuit, excluding the resistance of the plasma discharge, the capacitance and inductance is not constant in the time and the frequency-dependent (These values are used experimental value).

V. The PPT onboard the 1st PROITERES

We confirmed the validity of the numerical calculation by compared with experimental and calculated results with the PPT onboard the 1st PROITERES. Table 3 shows condition with the experiment and the numerical calculation.

Table 3. Experimental and calculated conditions of the PPT onboard the 1st PROITERES.

Cavity room	Length	10.0 mm
	Diameter	1.0 mm
Nozzle	Length	23.0 mm
	Diameter	20.0 mm
Capacitance		1.5 μF
Charging voltage		1,800 V
Inductance		0.35 μH
Resistance		0.05 Ω

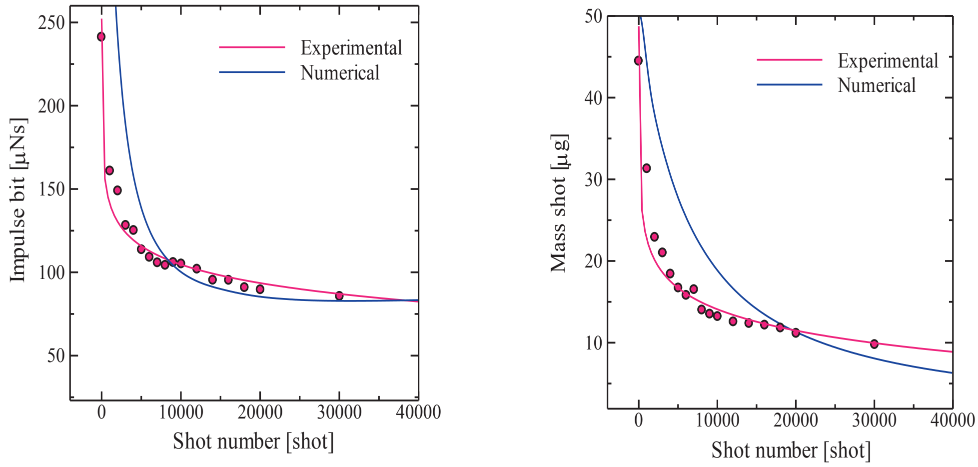

(a) Impulse bit vs shot number characteristic **(b) Mass shot vs shot number characteristic**

Figure 13. Comparison of operation by 40,000 shots.

Figure 13 shows comparison of the numerical calculation and the experiment results of an impulse bit and a mass shot by 40,000 shots operation. As shown in the figure, both the impulse bit and the mass shot of the numerical calculation results were lower than the experiment results over 10,000-20,000 shots, but it shows similar tendency. The numerical calculation was repeatedly performed in an ablation mass by constant ratio in axial direction. However, the ablation mass near the cathode in the experiment was smaller than that near the anode. This is expected the cause.

VI. The PPT onboard the 2nd PROITERES

A. Numerical calculation by changing cavity length and diameter

Numerical simulation of 400 shots operation by changing cavity length and diameter was performed for high-power PPT onboard the 2nd PROITERES satellite. Tables 4 and 5 show the condition of numerical calculation by changing cavity length and diameter. Figures 14 and 15 show the results of numerical calculation.

Table 4. Condition of numerical calculation by changing cavity length.

Cavity room	Length	10.0, 15.0, 20.0, 25.0 mm
	Diameter	4.0 mm
Nozzle	Length	19.0 mm
	Diameter	20.0 mm
Capacitance		19.5 μF
Charging voltage		1,800 V
Inductance		0.35 μH
Resistance		0.024 Ω

Table 5. Condition of numerical calculation by changing cavity diameter.

Cavity room	Length	10.0 mm
	Diameter	2.4, 3.0, 4.0, 5.0 mm
Nozzle	Length	19.0 mm
	Diameter	20.0 mm
Capacitance		19.5 μF
Charging voltage		1,800 V
Inductance		0.35 μH
Resistance		0.024 Ω

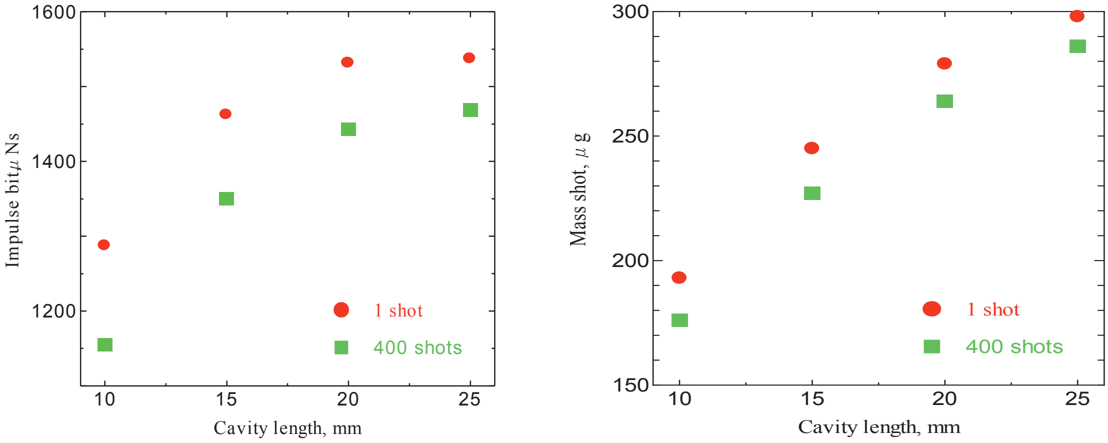

(a) Impulse bit vs cavity length characteristic **(b) Mass shot vs cavity length characteristic**

Figure 14. Results of numerical calculation by changing cavity length.

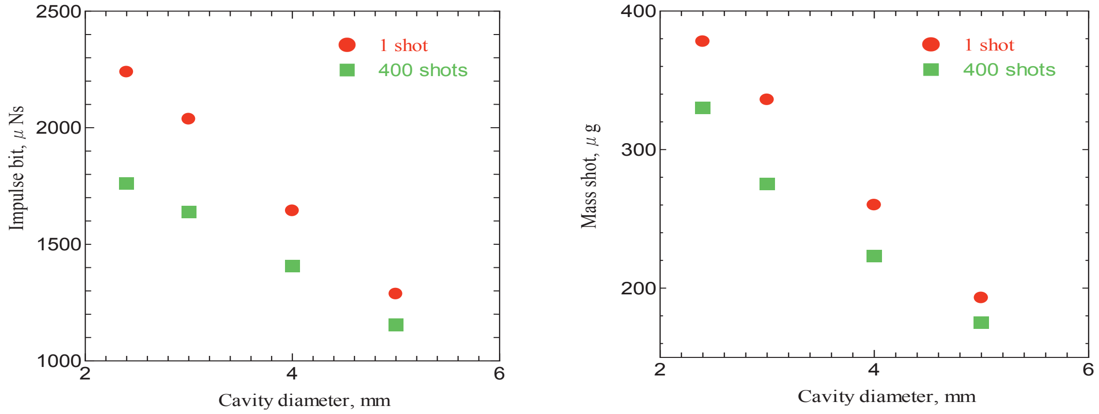

(a) Impulse bit vs cavity diameter characteristic **(b) Mass shot vs cavity diameter characteristic**

Figure 15. Results of numerical calculation by changing cavity diameter.

B. Numerical calculation by changing resistance

The PPT system has a Power Processing Unit (PPU) onboard a satellite for operation. Figure16 shows photo of the PPU onboard the 1st PROITERES. Table 6 shows specification of the PPU onboard the 1st PROITERES. In the 2nd PROITERES, the PPU is planned to be placed just behind the PPT head, resulting in very small resistance of the circuit. We set resistance values of 3 types and performed numerical calculation. Table 7 shows the condition of numerical calculation. Figure 17 shows the results of numerical calculation.

The maximum impulse bit was 2,260 μNs at the lowest resistance value of 0.005 Ω. The input power to plasma, as increasing energy transport efficiency resulting in increasing electron temperature and pressure, decreasing resistance value. Also, it is caused that the mass shot increases with raising ablation mass per shot by raising electron temperature or pressure. Their results are expected because of the place of the PPU just behind the PPT head.

Figure 16. The PPU onboard the 1st PROITERES.

Table 6. Specification of the PPU.

Mass		710 g
Size		100 × 100 × 50 mm
Power consumption		5 W
Input voltage		DC 12 V±10 %
Charge time		1.0 s
Output voltage	to CAP	1,800 V
	to Ignitor	2.25, 2.7 kV
Operating frequency		Optional

Table 7. Condition of the numerical calculation.

Cavity room	Length	25.0 mm
	Diameter	4.0 mm
Nozzle	Length	19.0 mm
	Diameter	20.0 mm
Capacitance		19.5 μF
Charging voltage		1,800 V
Inductance		0.35 μH
Resistance		0.005, 0.01, 0.024 Ω

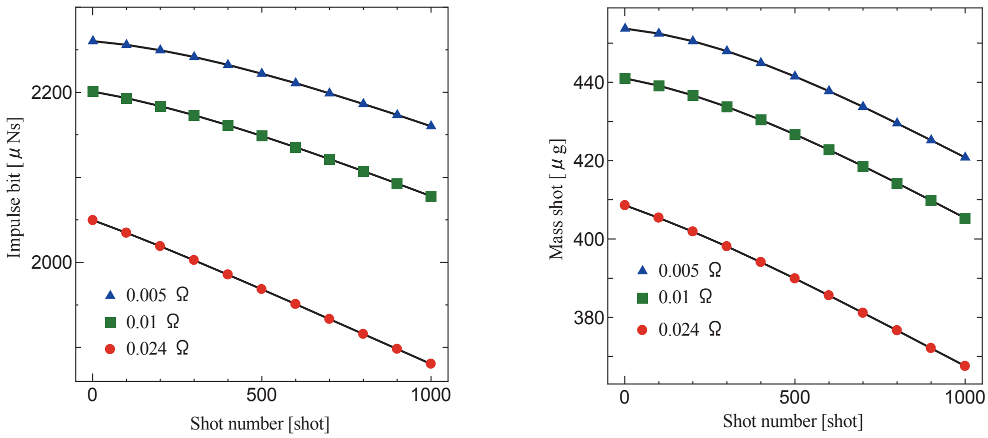

(a) Impulse bit vs shot number characteristic **(b) Mass shot vs shot number characteristic**

Figure 17. Results of numerical calculation by changing resistance values.

C. Numerical calculation by changing charging voltage

The 2nd PROITERES satellite aims at powered-flight with longer distance, i.e. changing 200-400 km in altitude on near-earth orbits, than that of the 1st PROITERES. Therefore, we must improve performance of PPT head itself. Then, the numerical calculation was performed by changing charging voltage. Table 8 shows the condition of numerical calculation. Figure 18 shows the results of numerical calculation by changing charging voltage. The results indicate that the impulse bit and the mass shot increases with increasing charging voltage. The maximum impulse bit was 2,589 μNs at a charging voltage of 2,000 V.

Table 8. Condition of the numerical calculation.

Cavity room	Length	25.0 mm
	Diameter	4.0 mm
Nozzle	Length	19.0 mm
	Diameter	20.0 mm
Capacitance		19.5 μF
Charging voltage		1,500, 1,600, 1,700, 1,800, 1,900, 2,000 V
Inductance		0.35 μH
Resistance		0.024 Ω

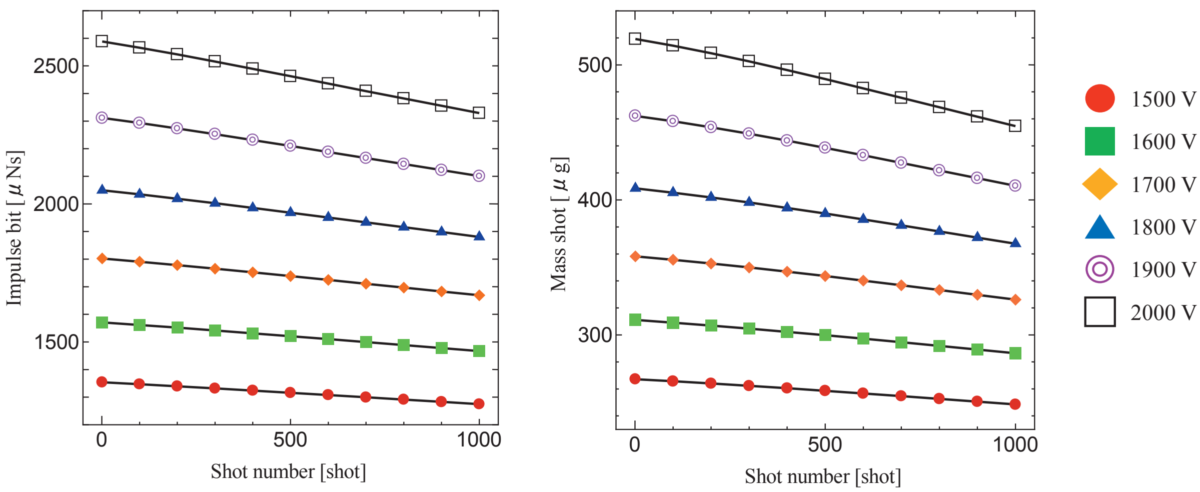

(a) Impulse bit vs shot number characteristic **(b) Mass shot vs shot number characteristic**

Figure 18. Results of numerical calculation by changing charging voltage.

VII. Conclusion

We confirmed the validity of numerical calculation by compared with experimental results and numerical calculation ones for the PPT onboard the 1st PROITERES.

1) The calculated one-shot performance was same as the experimental one. The maximum impulse bit was 250 μNs at the numerical calculation.
2) Both the impulse bit and the mass shot of the results of numerical calculation were lower than the results of experiment over 10,000-20,000 shots.

The numerical calculation of the PPT onboard the 2nd PROITERES was performed.

1) From the calculated results by changing cavity length and diameter, the impulse bit and mass shot were increased when cavity length was long and cavity diameter was small. The maximum impulse bit of about 1,500 μNs was predicted with a cavity length of 25 mm. The maximum impulse bit around 2,250 μNs was predicted with a cavity diameter of 2.4 mm.
2) From the calculated results by changing circuit resistance values, the impulse bit and the mass shot were increased at low resistance values. The maximum impulse bit was 2,260 μNs at the lowest resistance value of 0.005 Ω.
3) From the results by changing charging voltage, the impulse bit and the mass shot were increased at high charging voltage. The maximum impulse bit was 2,589 μNs at a charging voltage of 2,000 V.

Finally, the electrothermal PPT systems of 2-35 J for nano/small satellites will be commercialized by High-Serve Inc. and OIT in this R&D programs.

References

[1]Ikeda, T., Yamada, M., Shimizu, M., Fujiwara, T., Tahara, H., and Satellite R&D Team of Students and Faculty Members of OIT," Research and Development of an Attitude Control System for Osaka Institute of Technology Electric-Rocket-Engine onboard Small Space Ship," *27th International Symposium on Space Technology and Science*, Tsukuba, Japan, 2009, Paper No. ISTS 2009-s-02f.

[2]Takagi, H., Yamamoto, T., Ishii, Y., and Tahara, H.," Performance Enhancement of Electrothermal Pulsed Plasma Thrusters for Osaka Institute of Technology Electric-Rocket-Engine onboard Small Space Ship," *31st International Electric Propulsion Conference*, University of Michigan, Ann Arbor, Michigan, USA, 2009, Paper No. IEPC-2009-254.

[3]Ozaki, J., Ikeda, T., Fujiwara, T., Nishizawa, M., Araki, S., Tahara, H., and Watanabe, Y.," Development of Osaka Institute of Technology Nano-Satellite "PROITERES" with Electrothermal Pulsed Plasma Thrusters," *32nd International Electric Propulsion Conference*, Kurhaus, Wiesbaden, Germany, 2011, Paper No. IEPC-2011-035.

[4]Tahara, H., Ishii, Y., Tanaka, M., Naka, M., and Watanabe, Y.," Flowfield Calculation of Electrothermal Pulsed Plasma Thrusters for the PROITERES Satellite," *32nd International Electric Propulsion Conference*, Kurhaus, Wiesbaden, Germany, 2011, Paper No. IEPC-2011-037.

[5]Egami, N., Matsuoka, T., Sakamoto, M., Inoue, Y., and Ikeda T.," R&D,Launch and Initial Operation of the Osaka Institute of Technology 1st PROITERES Nano-Satellite with Electorothermal Pulsed Plasma Thrusters and Development of the 2nd satellite," *33nd International Electric Propulsion Conference*, George Washington University, USA, 2013, Paper No. IEPC-2013-100.

[6]Kamimura, T., Yamasaki, K., Egami, N., Matsuoka, T., Sakamoto, M., Inoue, Y., Ikeda, T., and Tahara, H., "Final Checking Process and Launch of the Osaka Institute of Technology 1st PROITERES Nano-Satellite Using Indian PSLV Rocket C-21", *29th International Symposium on Space Technology and Science*, Nagoya, Japan, 2013, Paper No. ISTS 2013-f-48p.

[7]Fujita, R., Uetsuji, Y., Tahara, H., "Research and development of the Osaka Institute of Technology PROITERES small-satellite structure system", *Asian Conference on Mechanics of Functional Materials and Structures*, Nara, Japan, 2014, Paper No. (923425)S.

[8]Muraoka, R., Kisaki, S., Tanaka, M., Tahara, H., and Wakizono, T., "Research and Development of Osaka Institute of Technology PROITERES Nano-Satellite Series with Electric Rocket Engines," *33nd International Electric Propulsion Conference*, George Washington University, USA, 2013, Paper No. IEPC-2013-103.

[9]Fujita, R., Muraoka, R., Hunnjun, C., Kisaki, S., Tanaka, T., and Tahara, H., Wakizono, T., "Development of Electrothermal Pulsed Plasma Thruster Systems onboard Osaka Institute of Technology PROITERES Nano-Satellites", *AIAA Propulsion and Energy Forum and Exposition 2014*, Cleveland Convention Center, USA, 2014, Paper No. AIAA-2014-3610.

[10]Hunnjun, C., Kisaki, S., Muraoka, R., Tanaka, M., Tahara, H., and Wakizono, T.," Performance Prediction of Electrothermal Pulsed Plasma Thruster Systems onboard Osaka Institute of Technology PROITERES Nano-Satellite Series," *33nd International Electric Propulsion Conference*, George Washington University, USA, 2013, Paper No. IEPC-2013-102.

[11]Tanaka, M., Kisaki, S., Ikeda, T., and Tahara, H., "Research and Development of Pulsed Plasma Thruster Systems for Nano-Satellites at Osaka Institute of Technology", *8th IEEE Vehicle Power and Propulsion Conference*, Olympic Parktel, Seoul, Korea, 2012, Paper No. SS01-0300.

[12]Tanaka, M., Naka, M., Tahara, H., and Watanabe, Y., "Flowfield Calculation of Electrothermal Pulsed Plasma Thrusters for Nano-Satellite PROITERES", *28th International Symposium on Space Technology and Science*, Okinawa Convention Center, Okinawa, Japan, 2011, ISTS 2011-b-61p.